State-dependent firing determines intrinsic dendritic Ca²⁺ signalling in thalamocortical neurons

Adam C. Errington[1], **John J. Renger**[2], **Victor N. Uebele**[2], and **Vincenzo Crunelli**[1]

[1] Neuroscience Division, School of Biosciences, Cardiff University, Cardiff, UK

[2] Merck Research Laboratories, West Point, Pennsylvania, USA

Abstract

Activity-dependent dendritic Ca^{2+} signals play a critical role in multiple forms of non-linear cellular output and plasticity. In thalamocortical neurons, despite the well-established spatial separation of sensory and cortical inputs onto proximal and distal dendrites respectively, little is known about the spatio-temporal dynamics of intrinsic dendritic Ca^{2+} signalling during the different state-dependent firing patterns that are characteristic of these neurons. Here we demonstrate that T-type Ca^{2+} channels are expressed throughout the entire dendritic tree of rat thalamocortical neurons and that they mediate regenerative propagation of low threshold spikes, typical of, but not exclusive to sleep states, resulting in global dendritic Ca^{2+} influx. In contrast, actively backpropagating action potentials, typical of wakefulness, result in smaller Ca^{2+} influxes that can temporally summate to produce dendritic Ca^{2+} accumulations which are linearly related to firing frequency but spatially confined to proximal dendritic regions. Furthermore, dendritic Ca^{2+} transients evoked by both action potentials and low threshold spikes are shaped by Ca^{2+} uptake by sarco/endoplasmic reticulum Ca^{2+} ATP-ases, but do not rely upon Ca^{2+}-induced Ca^{2+} release. Our data demonstrate that thalamocortical neurons are endowed with intrinsic dendritic Ca^{2+} signalling properties that are spatially and temporally modified in a behavioural state-dependent manner, and suggest that backpropagating action potentials faithfully inform proximal sensory but not distal corticothalamic synapses of neuronal output whereas corticothalamic synapses only "detect" Ca^{2+} signals associated with low threshold spikes.

Keywords

Introduction

Active dendritic conductances are critical for many complex cellular activities including co-incidence detection, dendritic Ca^{2+} spike initiation, local synaptic integration and synaptic plasticity (Häusser et al., 2000, Holthoff et al., 2006). In particular, they permit active backpropagation of axo-somatically initiated action potentials (bAPs) to different extents throughout the dendritic trees of various neurons (Magee and Johnson, 1995; Spruston et al. 1995; Bischoberger and Jonas, 1997; Häusser et al., 1995; Stuart et al., 1993, 1997;

Markram et al., 1995; Schiller et al., 1995) with significant physiological consequences. For example, the timing relationship between bAPs and near co-incident excitatory synaptic activity has been demonstrated to confer a range of non-linear dendritic signalling properties (Kampa et al., 2007, Holthoff et al., 2006).

Sensory thalamocortical (TC) neurons sit in a pivotal position for signal integration within thalamocortical circuits since they receive both sensory and corticothalamic (CT) afferents (Sherman and Guillery, 1996). Significantly, these glutamatergic inputs are spatially separated in the TC neuron dendritic tree, with sensory input arriving on stem dendrites close to the first dendritic branch point ($< 50 \mu$m) and CT fibers forming synapses mainly onto sparsely spiny intermediate or distal dendrites ($\sim$ 70-150 μm) (Sherman and Guillery, 1996; Wilson et al., 1984; Liu et al., 1995). Indeed, up to 50% of all synaptic connections onto TC neurons are formed by CT afferents onto distal dendrites (Wilson et al., 1984; Liu et al., 1995). Furthermore, GABAergic afferents onto TC neurons are also differently distributed across their dendrites, with local interneuronal inputs preferentially targeting perisomatic regions and reticular thalamic neurons (nRT) making synapses throughout the entire dendritic tree.

Despite such intricate dendritic synaptic architecture, however, our understanding of the cellular physiology of TC neurons is still restricted to a mainly somatic view. In particular, the non-linearity in TC neuron output that is linked to a behavioural state-dependent recruitment of T-type Ca^{2+} channels (Llinas and Jahnsen, 1982; Steriade et al., 1993) and expression of low threshold Ca^{2+} spikes (LTSs) has only been studied in the soma and very proximal dendrites. As such, the presence T-type Ca^{2+} channels, as well as voltage-gated Na^+ and K^+ channels and high voltage activated (HVA) Ca^{2+} channels in TC neuron dendrites has previously been demonstrated by several imaging, electrophysiological and anatomical studies (Zhou et al., 1997; Budde et al., 1998; Munsch et al. 1997; Williams and Stuart, 2000). However, these studies were limited to somatic and proximal ($< 50 \mu$m) dendritic regions and although computer simulations suggest that high levels of T-type Ca^{2+} conductance throughout the dendritic tree are necessary for LTS-dependent activities (Rhodes and Llinas, 2005; Destexhe et al., 1998; Emri et al., 2000), no experimental confirmation of this prediction has been made.

Here, by investigating the dynamics of intrinsic dendritic Ca^{2+} signalling across the full TC neuron dendritic tree, we found that LTSs generate near instantaneous *global* Ca^{2+} influx whereas backpropagating APs (bAPs) evoke Ca^{2+} transients that temporally summate to produce Ca^{2+} accumulations which are linearly related to AP frequency but are spatially restricted to proximal dendrites.

Materials and Methods

Electrophysiology

Coronal slices (300 μm) containing the dorsal lateral geniculate nucleus (dLGN) were prepared from P21-24 Wistar rats of either sex in chilled (1-3°C) cutting solution bubbled with carbogen (95% O_2 / 5% CO_2) (mM: 60 Sucrose, 85 NaCl, 2.5 KCl, 1 $CaCl_2$, 2 $MgCl_2$, 1.25 NaH_2PO_4, 25 $NaHCO_3$, 25 D-glucose, 3 kynurenic acid, 0.045 indomethacin) in accordance with the Home Office Animals (Scientific Procedures) Act 1986, UK. Slices were stored for 20 minutes at 35 °C in sucrose containing solution and then maintained at room temperature in artificial CSF (aCSF) (mM: 125 NaCl, 2.5 KCl, 1 $CaCl_2$, 2 $MgCl_2$, 1.25 NaH_2PO_4, 25 $NaHCO_3$, 25 D-glucose, 305 mOsm) and used within 4-6 hours. For recording, slices were transferred to a submersion chamber continuously perfused with warmed (35 °C) aCSF (mM: 125 NaCl, 2.5 KCl, 2 $CaCl_2$, 1 $MgCl_2$, 1.25 NaH_2PO_4, 25 $NaHCO_3$, 25 D-glucose, 305 mOsm) at a flow rate of 2-2.5 ml.min^{-1}. Somatic whole-cell

patch clamp recordings were performed on TC neurons (visually identified by infrared videomicroscopy) using pipettes with resistances of 4-6 MΩ when filled with internal solution containing (mM) 135 K-methylsulfonate, 10 HEPES, 10 Na-phosphocreatine, 4 $MgCl_2$, 4 Na-ATP, 0.4 Na-GTP (pH 7.3, 300 mOsm) supplemented with Alexa Fluor 594 (25 μM) and Fluo 5F (300 μM) or Fluo 4FF (500 μM) (Invitrogen Molecular Probes, UK) for Ca^{2+} imaging. Electrophysiological data was acquired at 20 kHz and filtered at 6 kHz using a Multiclamp 700B patch clamp amplifier and pClamp 10 software (Molecular Devices, USA). Series resistance at the start of experiments was between 11-15 MΩ and varied   20% during recordings.

Backpropagating action potentials (bAPs) and LTS were evoked by somatic current injection from membrane potentials of approximately −50 mV and −70 mV (held by constant d.c. injection), respectively, using either 1-1.5 nA, 2 ms square pulses (bAPs) or 100-140 pA, 50 ms pulses (LTS). bAP trains were evoked using the same pulse delivered at frequencies between 10 and 120 Hz for 500-700 ms and stimulus trials were delivered with 10-20 s intervals. Focal dendritic application of drugs was achieved by placing a 'puffer' patch pipette containing HEPES buffered aCSF (mM: 145 NaCl, 2.5 KCl, $CaCl_2$ 2, $MgCl_2$ 1, HEPES 10, D-glucose 25, pH 7.3) close (~ 10-15 μm) to the dendrite of interest using IR-scanning Dodt contrast. Gentle pressure was applied using a syringe and data collected during drug application. Trial experiments were performed using blank aCSF supplemented with Alexa 594 to confirm the lack of effect of vehicle solution on Ca^{2+} transients and spatial distribution of the 'puff'. During the course of the experiment the diffusion of locally applied drugs was restricted to approximately 60 μm. Local synaptic stimulation by activation of putative CT axons was achieved in the presence of the $GABA_A$ antagonist SR-95531 (10 μm) using a glass pipette filled with HEPES buffered aCSF (as above) placed within 15 μm of a selected distal dendrite. Trains of 3 small (0.1-10 V), brief (200 μs) stimuli were delivered at intervals of 30 ms.

Imaging

Two photon laser scanning microscopy (2P-LSM) was performed using a Prairie Ultima (Prairie Technologies, Madison, USA) microscope powered by a Ti:sapphire pulsed laser (Chameleon Ultra II, Coherent, UK) tuned to λ=810 nm. Image acquisition was controlled using Prairieview software and laser intensity was modified using a Pockels cell electro-acoustic modulator (ConOptics, USA). Prior to commencing imaging experiments neurons were loaded with indicators for 20 minutes to allow complete equilibration and reduce nonlinearities during stimulus evoked Ca^{2+} influx. Dendrites were then imaged using a 40×/0.8NA objective lens and fluorescence signals from Alexa 594 (red, R) and Fluo (green, G) indicators were collected simultaneously in the epicollection mode using multialkali photomultiplier tubes (Hamamatsu Photonics, Hamamatsu, Japan). Dendritic fluorescence signals were recorded by performing linescans (500 Hz, Fig. 1B) across dendrites at selected regions of interest (0.042 μm per pixel, 7.2 μs pixel dwell time). For calculation of distance dependent differences in AP evoked changes in intracellular Ca^{2+} (ΔCa^{2+}), dendrites were selected that were limited to a single optical plane (20 μm Z variance). Distances were approximated by measuring along the dendrite from the somatic centre to the dendritic ROI on a two dimensional maximum intensity projection of each neuron (Fig. 1A). Maximum intensity projections were constructed from Z series of 120-150 images (512 pixels, 0.66 μm per pixel) taken with 1μm focal steps. To prevent photodamage during linescans most data presented represent averages of 10 trials but in order to obtain signal to noise (S/N) ratios sufficient for successful exponential fitting some experiments required 20 repetitions (e.g. single APs). Fluorescence signals were measured by integration of the signal over a region where the intensity of the red channel was greater than 80 % of the peak fluorescence (white bars, Fig. 1B). Offsets from the photomultipliers and preamplifier were measured in the dark

and subtracted from all measurements. No other background correction was applied as autofluorescence is insignificant in 2P-LSM and care was taken to minimise indicator spill into the extracellular space during patching. The ratio of the Ca^{2+} sensitive fluorescence signal (G) to the Ca^{2+} insensitive signal (R) was used as a measure of stimulus evoked dendritic $[Ca^{2+}]$. The amplitude of the stimulus evoked dendritic $\Delta[Ca^{2+}]$ $\Delta G/R$ was determined by subtracting baseline G/R values (50 ms period before stimulus) from the peak G/R signal (20-50 ms interval). To estimate indicator saturation for Fluo 5F and Fluo 4ff, we measured G/R_{max} (0.7 and 0.95) in 10 mM Ca^{2+} and G/R_{min} (0.02 and 0.05) in 10 mM EGTA in a patch pipette in our microscope. During experiments typical maximum $\Delta G/R_{signals}$ were 0.23 and 0.1 for Fluo 5F and Fluo 4ff and $\Delta G/R_{rest}$ was 0.05 and 0.04 resulting in nonlinearity errors $[\Delta G/R_{signals}/(\Delta G/R_{max} - \Delta G/R_{rest})]$ of 36% and 9%, respectively. Although the maximum nonlinearity error associated with 300 µM Fluo 5F measurements is larger than would typically be desired we found that this was the best Ca^{2+} indicator and concentration to measure the relatively small dendritic AP evoked signals and larger LTS evoked signals in the same neurons in the near-linear range. Therefore, in experiments where $\Delta[Ca^{2+}]$ evoked by different firing modes or firing frequencies were compared or decay time constants were measured, effects of saturation were routinely compensated by correcting traces using the equation (Scheuss et al., 2006):

$$(G/R)_{corr} = (G/R) / (1 - (G/R) / (G/R)_{max}) \quad (1)$$

After correction fluorescence signals (G/R) were converted into Ca^{2+} concentrations using:

$$\left[Ca^{2+}\right]/K_d = (G/R) - (G/R)_{min}/(G/R)_{max} - (G/R)_{min} \quad (2)$$

Under our conditions the K_d of Fluo 5F was measured as 0.8 µM, which is similar to previously reported values (Yasuda et al., 2003) and we used values reported in the literature to calculate Ca^{2+} concentration for Fluo 4ff experiments (8.1 µM). The exogenous buffer capacity (K_B) was estimated using the incremental Ca^{2+} binding ratio (Neher and Augustine, 1992):

$$K_B = K_d[B]_{total} / \left(K_d + \left[Ca^{2+}\right]_0\right)\left(K_d + \left[Ca^{2+}\right]_0 + \Delta\left[Ca^{2+}\right]\right) \quad (3)$$

where $[B]_{total}$ is the total concentration of added buffer, $[Ca^{2+}]_0$ is the resting calcium level and $\Delta[Ca^{2+}]$ is the evoked Ca^{2+} increment.

Analysis

Linescan analysis was performed offline using Metamorph software (Molecular Devices, USA). Decay time contants (τ_{decay}) were measured by fitting mono-exponentials (Prizm 5, Graphpad Software, USA) to the decay phase of $\Delta[Ca^{2+}]$ with fits constrained by peak G/R and baseline G/R values. In thin dendrites, such as those found in TC neurons, AP evoked Ca^{2+} dynamics is well described by a single compartment model with the transient amplitude determined by the amount of Ca^{2+} influx and the decay reflecting the rate of Ca^{2+} extrusion. To determine if these factors are modulated by activity in TC neurons, $\Delta[Ca^{2+}]$ measured during tonic firing at different frequencies were compared with those predicted based upon the dynamic properties of single spike evoked $\Delta[Ca^{2+}]$. During a stimulus train, such as tonic AP firing, the steady-state Ca^{2+} level is attained when influx and extrusion are balanced:

$$\Delta\left[Ca^{2+}\right]_{steady-state} = \Delta\left[Ca^{2+}\right]_{AP} \tau \upsilon_{AP} \quad (4)$$

where $\Delta[Ca^{2+}]_{AP}$ is the $\Delta[Ca^{2+}]$ per action potential, τ is the measured decay time constant for a single bAP evoked $\Delta[Ca^{2+}]$ and υ_{AP} is the inverse of the interspike interval (Helmchen et al., 1996; Scheuss et al., 2006). These analyses were performed on data that were corrected for nonlinearity as previously described because time integrals of $\Delta[Ca^{2+}]$ can be affected significantly by indicator saturation. Some predictions of activity evoked dendritic Ca^{2+} changes were made using the linear sum of the exponentials fitted to single AP transients offset to match the relative spike timing.

All averaged data are shown as mean $\pm$ s.e.m. and n refers to the number of cells tested unless otherwise indicated. Statistical significance was verified using tests indicated in the text with $\alpha < 0.05$.

Results

Spatial distribution of LTS and AP evoked Ca^{2+} transients in TC neuron dendrites

We used a combination of whole cell recording and 2 photon laser scanning microscopy to examine Ca^{2+} signals evoked by bAP and LTS throughout the entire dendritic tree of TC neurons of the dLGN. Neurons were loaded through a patch pipette with a green fluorescent Ca^{2+} sensitive indicator (Fluo 5F or Fluo 4FF) and a red Ca^{2+} insensitive morphological tracer (Alexa Fluor 594) revealing short (~150 µm), spherically radiating (stellate) and mostly aspiny dendrites (Fig. 1A) typical of rodent TC cells. Firstly, we investigated dendritic LTS evoked Ca^{2+} influx ($\Delta[Ca^{2+}]_{LTS}$) in TC neurons as a function of distance from the soma. By evoking LTS using brief depolarizing current injection at the soma (V_m: -72.4 ± 0.3 mV, n = 8) whilst simultaneously performing linescans at various dendritic locations, we observed a *global* Ca^{2+} influx throughout the entire TC neuron dendritic tree (Fig. 1A,C1,F). $\Delta[Ca^{2+}]_{LTS}$ were relatively fast rising (~ 30-40 ms), even in the presence of added Ca^{2+} buffer, were temporally co-incident with the somatically recorded LTS and occurred quasi-synchronously throughout the entire dendritic tree (Fig. 1F, Video S1). Imaging pairs of distal (100-110 µm) dendritic locations revealed simultaneous evoked $\Delta[Ca^{2+}]_{LTS}$ whose amplitudes and decay time constants were nearly identical (n = 4 pairs from 3 neurons, Fig. 1F). On average, pooled data from all our experiments showed that measured $\Delta[Ca^{2+}]_{LTS}$ were ~1.6 times larger (ΔG/R proximal: 0.153 ± 0.01, n = 37; ΔG/R distal: 0.247 ± 0.01, n = 21, P < 0.001, unpaired t-test) and decayed more rapidly (τ_{decay} proximal: 185.7 ± 8.3ms, n = 37; τ_{decay} distal: 97.4 ± 8.4ms, n = 21, P < 0.001) in thinner distal dendrites compared with proximal stem or secondary dendrites (Fig. 1C1,E). However, complications can arise where one wishes to compare $\Delta[Ca^{2+}]$ in different parts of the dendritic tree since Ca^{2+} indicator concentration may not be equal at all sites. Thus, if dye concentration is lower at distal sites $\Delta[Ca^{2+}]$ may appear larger (and faster) because of reduced exogenous buffering. During our experiments we allowed a loading period of 20 minutes and experimentation time of approximately 30 minutes. After this time the health of TC neurons deteriorates and changes in electrical properties become apparent presumably due to dialysis of the cell interior. Although we varied the tested dendritic locations randomly over time for different neurons, it is possible that equal dye concentrations are not achieved in the extensively branched fine distal dendrites over the duration of our experiments or that the dye is distributed as a steady-state concentration gradient along the dendrite. To account for this possibility, we compared the time integrals (Aτ) of $\Delta[Ca^{2+}]_{LTS}$ as a function of distance from the soma as this measurement is independent of buffer concentration (Helmchen et al., 1996). The time integrals of the $\Delta[Ca^{2+}]_{LTS}$ showed a uniform distribution along the dendritic axis (Fig. 1E) without significant differences between $\Delta[Ca^{2+}]$ in proximal and intermediate/distal dendrites. This analysis demonstrates that, even accounting for this possible source of experimental error, TC neurons have global all-or-none dendritic Ca^{2+} influx during LTS and that distal Ca^{2+} influx is, at least,

comparable to that observed proximally (not accounting for potential differences in surface area-to-volume ratios).

In marked contrast to $\Delta[Ca^{2+}]_{LTS}$, $\Delta[Ca^{2+}]$ resulting from single bAPs ($\Delta[Ca^{2+}]_{bAP}$) evoked by brief current pulses (1-1.5 nA, 2 ms) in the same TC neurons depolarized by dc injection (-51.7 ± 0.2 mV, n = 9) were spatially restricted to proximal regions of the dendritic tree (Fig. 1C2). Amplitudes of $\Delta[Ca^{2+}]_{bAP}$ in proximal dendrites were 7 to 10 times smaller than those of $\Delta[Ca^{2+}]_{LTS}$ (P < 0.001, n = 6) and showed marked attenuation with increasing distance from the soma (length constant ~ 24 μm, black circles, Fig. S1A). Since APs that crown an LTS in rodent TC neurons have typical instantaneous frequencies of approximately 200-250 Hz, we also tested the possibility that distal $\Delta[Ca^{2+}]$ observed during LTS were the result of dendritic Ca^{2+} spikes triggered by bursts of bAPs when TC cells fire above a certain 'critical' frequency as has been demonstrated in other neurons (Larkum et al. 1999, 2007; Kampa and Stuart 2006). As for $\Delta[Ca^{2+}]_{bAP}$ and unlike $\Delta[Ca^{2+}]_{LTS}$, $\Delta[Ca^{2+}]$ evoked by a burst of 3 APs at 200 Hz ($\Delta[Ca^{2+}]_{3APs}$) were strongly dependent upon distance from the soma (Fig. 1C3). At proximal locations, the amplitude of $\Delta[Ca^{2+}]_{3APs}$ was $\Delta G/R = 0.06 \pm 0.007$ but this dropped strikingly with distance (length constant ~ 43 μm, light grey diamonds, Fig. S1A) such that in distal dendrites meaningful $\Delta[Ca^{2+}]_{3APs}$ were not observed (P < 0.001, n = 8)(Fig. 1C3). Together with the observation of considerable LTS-evoked fluorescence changes in distal dendrites, the lack of any Ca^{2+} increase evoked by 3 bAPs appears to rule out poor S/N ratio (Fluo 5F; K_d ~ 0.8 μM) as a factor that might confound our ability to observe evoked $\Delta[Ca^{2+}]$ in thin dendrites during single bAPs.

Given that *in vivo* during wakefulness TC neurons do not typically fire single APs or short high frequency bursts of APs but instead produce sustained 'tonic' AP firing, we also characterised spatial differences in dendritic Ca^{2+} elevations during a train of 15 APs at 30 Hz (bAP$_{30Hz}$). In proximal dendrites, $\Delta[Ca^{2+}]_{bAP30Hz}$ reached plateau levels that were marginally less than the peak $\Delta[Ca^{2+}]$ observed during LTSs, but at distal locations even relatively long trains of 15 spikes were unable to produce significant Ca^{2+} elevations above rest, seemingly confirming the inability of APs to effectively backpropagate into distal dendrites (Fig. 1C4,D).

LTSs regeneratively propagate throughout the entire TC neuron dendritic tree

It is well established that actively backpropagating Na^+-mediated APs can produce transient increases in dendritic $[Ca^{2+}]$ in many neurons. Therefore, we next tested the extent to which dendritic $\Delta[Ca^{2+}]$ in TC neurons, evoked by either bAPs or LTS, relied upon active backpropagation of Na^+ spikes. To do this we firstly made a quantitative comparison between $\Delta[Ca^{2+}]_{LTS}$ (2.3 ± 0.1 APs/burst, range 1-5, n = 11) and $\Delta[Ca^{2+}]$ generated by a similar number of bAPs at comparable frequencies in the same TC neurons (1-5 bAPs, 200 Hz). We found that the amplitudes of $\Delta[Ca^{2+}]$ evoked by high frequency bAP bursts were linearly proportional to the number of bAPs (Fig. 2A) whereas their decay time constants (τ_{decay}) were independent of bAP number (P > 0.05)(Fig. 2B). Furthermore, despite the fact that $\Delta[Ca^{2+}]$ evoked by bursts of 3 or 5 bAPs were nearly identical to those predicted by the linear sum of $\Delta[Ca^{2+}]$ evoked by single bAPs (P > 0.05) they were always significantly less than $\Delta[Ca^{2+}]_{LTS}$ (3bAPs: P < 0.001, 5bAPs: P < 0.01, n = 11, one-way ANOVA)(Fig. 2B) recorded at the same proximal dendritic locations. Thus, the $\Delta[Ca^{2+}]$ observed during LTS did not result from high frequency AP dependent Ca^{2+} spike intiation as is the case in other neurons types. The sizeable supra-linearity of $\Delta[Ca^{2+}]_{LTS}$ compared with bursts of evoked APs alone (~3 fold for bursts of 3 APs) implied that $\Delta[Ca^{2+}]_{LTS}$ incorporated Ca^{2+} influx via a mechanism that does not rely upon Na^+ mediated bAPs. To test this hypothesis, we blocked bAPs using bath application of tetrodoxin (TTX). In the presence of TTX (0.5 μM) $\Delta[Ca^{2+}]_{LTS}$ were as predicted, observed at both proximal and distal (>100 μm) dendritic

locations suggesting that LTSs are able to propagate throughout TC neuron dendrites. In proximal dendrites, the absence of APs resulted in a small but significant reduction of the $\Delta[Ca^{2+}]_{LTS}$ compared to pre-treatment levels (G/R CONT: 0.156 ± 0.016, TTX: 0.107 ± 0.016, $P < 0.01$, n = 9, paired t-test)(Fig. 3A2). Interestingly, the decrease in amplitude of $\Delta[Ca^{2+}]_{LTS}$ was similar in magnitude to the Ca^{2+} signal evoked by 3 bAPs alone (n = 11 different cells)(see Fig. 2A,B). This implies that whilst LTSs can produce dendritic $\Delta[Ca^{2+}]$ without bAPs, in regions of the dendritic arbor where bAPs effectively propagate they contribute to the overall $\Delta[Ca^{2+}]$ during burst firing. As expected however, at distal locations where bAPs fail to invade, we did not see a significant reduction in the amplitude of $\Delta[Ca^{2+}]_{LTS}$ in the presence of TTX (G/R CONT: 0.223 ± 0.017, TTX: 0.196 ± 0.025, $P > 0.05$, n = 9)(Fig. 3A3). In fact, comparison of the number of APs per LTS with the dendritic $\Delta[Ca^{2+}]_{LTS}$ revealed a correlation between the number of spikes and Ca^{2+} transient amplitude for proximal but not distal dendrites (Fig. S1B). Finally, in contrast to $\Delta[Ca^{2+}]_{LTS}$, TTX completely occluded Ca^{2+} elevations produced by trains of APs confirming that active backpropagation through voltage-gated Na^+ channels was absolutely necessary for these signals (Fig. 3A1). In fact, brief passive depolarisation of the electrotonically compact TC neurons in the presence of TTX using 3 ms voltages steps (60 mV) from -50 mV at 50 Hz (700 ms) to mimic AP trains did not result in significant $[Ca^{2+}]$ elevations above rest even in proximal dendrites (n = 3)(Fig. 3B2). This is consistent with previous dendritic recordings in TC neurons (Williams & Stuart, 2000; see their Fig. 5). In the presence of TTX, dendritic voltage changes in response to injection of an AP waveform at the soma were significantly smaller than those observed with actively backpropagating APs. Despite the fact that dendritic AP width is increased compared to the somatic spike this prolongation is insufficient to allow summation of the dendritic voltage responses at most physiological pertinent firing rates. Thus, the passive dendritic responses to our brief 60 mV steps are likely to be markedly decreased in amplitude compared with the soma and insufficient to activate HVA Ca^{2+} channels and permit Ca^{2+} entry. In contrast, when continuous 60 mV steps were applied for 700 ms the effects of passive depolarisation were sufficient to induce very large dendritic Ca^{2+} influx (Fig. 3B3). Note however the lag between the onset of the somatic voltage step and the onset of dendritic Ca^{2+} accumulation.

Linear summation of dendritic Ca^{2+} transients during tonic firing

As previously described, during wakefulness TC neurons typically fire prolonged trains of APs in response to integrated sensory and CT inputs and these can vary over a wide range of frequencies depending upon the level of synaptic excitation (typically up to 80 Hz). Therefore, we measured activity-dependent accumulation of Ca^{2+} in dendrites during APs trains at several physiologically relevant firing rates. We found that single bAPs evoked instantaneous δ-function like $\Delta[Ca^{2+}]$ (Fig. 4A) in proximal dendrites (20-30 μm) whose decay phases (τ_{decay}) were well fit by a mono-exponential function, consistent with description by a single compartment model where $\Delta[Ca^{2+}]$ amplitude (A) is a measure of near instantaneous Ca^{2+} influx and τ_{decay} reflects the rate of Ca^{2+} extrusion (Helmchen et al. 1996). Upon repetitive stimulation, using AP trains at different frequencies, dendritic Ca^{2+} accumulation reached a steady-state plateau level reflecting balance between Ca^{2+} influx per AP and Ca^{2+} extrusion. In TC neurons loaded with 300μM Fluo 5F we found a linear relationship between dendritic plateau Ca^{2+} concentration ($[Ca^{2+}]_{plat}$) and AP firing at frequencies up to 50 Hz (Fig. 4B). The time to reach steady state Ca^{2+} levels was not significantly different for bAP trains at 10, 30 or 50 Hz with mono-exponential fits to the rising phase of the signals giving time constants of 237.5 ± 18.42 ms, 234.1 ± 16.49 ms and 267.8 ± 17.84 ms respectively (Fig. 4F). Under our conditions the $[Ca^{2+}]$ levels at the end of 10, 30 and 50 Hz AP trains were approximately 0.042, 0.12 and 0.23 μM. A regression line fitted to mean $[Ca^{2+}]_{plat}$ versus AP frequency yielded a slope of 4.46 nM / Hz (Fig. 4G), a value that closely agrees with the mean proportionality constant Aτ (4.63 ± 0.36, n = 18)

calculated using the amplitude and τ_{decay} of single bAP evoked $\Delta[Ca^{2+}]$ for individual TC neurons. In addition, when expected $[Ca^{2+}]_{plat}$ levels, calculated using equation 4, were plotted against measured train-evoked Ca^{2+} elevations values did not deviate from equality, confirming a linear relationship under these conditions (Fig. 4D). Moreover, as expected for linearly superimposed transients we did not see significant (P > 0.05, n = 18, repeated measures ANOVA) differences between τ_{decay} for single bAPs (201.5 ± 17.6 ms) or trains at any of the tested frequencies (10 Hz, 223.1 ± 13.4 ms; 30 Hz, 226.6 ± 10.0 ms; 50 Hz, 224.9 ± 8.8 ms). These findings suggest that activity-dependent changes in Ca^{2+} extrusion, as have been demonstrated in other neurons (Scheuss et al., 2006), are not a feature of TC neuron dendritic Ca^{2+} signalling during tonic firing at physiological rates. Even during prolonged (5 s) trains of 250 APs at 50 Hz $[Ca^{2+}]_{plat}$ were not significantly larger (P > 0.05, n = 3) than those attained during our 700 ms stimulus trains and τ_{decay} were nearly identical (Fig. S2).

Nonetheless, elegant studies in CA1 hippocampal pyramidal neurons have revealed that activity-dependent changes in Ca^{2+} extrusion rate resulting in supralinear Ca^{2+} accumulations during AP trains are Ca^{2+}-dependent and can be masked by the addition of high levels of exogenous Ca^{2+} buffers (Scheuss et al., 2006). In our experiments, using Fluo 5F, we estimate an added buffer capacity of $K_B \approx 300$ and therefore cannot rule out the possibility that this could perturb normal Ca^{2+} dynamics during AP trains. We therefore performed experiments using the low affinity indicator Fluo 4ff (500 µM; K_D: 8.1 µM) and estimated $[Ca^{2+}]_{plat}$ during AP trains at 30, 60 and 120 Hz (Fig. S3). Under conditions of low added buffer ($K_B \approx 60$), we found that the linear relationship between Ca^{2+} and AP frequency in TC neurons was maintained up to 120 Hz (Fig. 4C). At 120 Hz, Ca^{2+} plateaus were very slightly larger than the expected level, based on Fluo 5F data, suggesting small non-linear accumulation of Ca^{2+} during very high frequency trains. However, even at 120 Hz we estimate that the plateau Ca^{2+} level remains less than 0.8 µM which is markedly lower than that observed in dendrites and spines of other neurons. In addition, even in the absence of significant levels of added buffer τ_{decay} of train evoked Ca^{2+} signals did not significantly differ with AP frequency (95-115 ms)(Fig. 4C and Fig. S3) and were relatively fast signifying that TC neuron dendrites may have robust mechanisms for Ca^{2+} clearance (i.e. high expression of sarco/endo plasmic reticulum Ca^{2+} ATP-ases (SERCA), plasma membrane Ca^{2+} ATP-ases (PMCA) and Na^+/Ca^{2+} exchanger and/or comparatively low endogenous buffering capacity).

Role of CICR and SERCA in TC neuron dendritic Ca^{2+} signalling

Previously, it has been suggested Ca^{2+} induced Ca^{2+} release (CICR) though ryanodine receptors (RyR) plays a pivotal role in supporting tonic firing in TC neurons (Budde et al., 2000). Given that dendritic $\Delta[Ca^{2+}]$ associated with single bAPs are typically insufficient to induce CICR and our previous experiments showed a linear relationship between spike frequency and dendritic Ca^{2+} build up we decided to assess the potential contribution of CICR from endoplasmic reticulum stores to bAP and LTS evoked $\Delta[Ca^{2+}]$ in TC neuron dendrites. Inclusion of ryanodine (20 µM) in the patch pipette solution to block RyR-mediated Ca^{2+} release did not produce significant changes in amplitude or τ_{decay} of $\Delta[Ca^{2+}]$ evoked in proximal dendrites by LTSs, single bAPs, 5 bAPs at 200 Hz and bAP trains (700 ms, 50 Hz) or in distal dendrites by LTSs (P > 0.05, n = 7-9) (Fig. 5A,B and Fig. S4) when compared to control neurons (n = 18). In the absence of activity dependent dendritic Ca^{2+} release we next sought to determine whether uptake into ER stores played a role in Ca^{2+} clearance during both LTSs and bAPs in TC neuron dendrites. In a separate group of neurons, inhibition of SERCA by bath application of cyclopiazonic acid (CPA, 10 µM) produced significant slowing of $\Delta[Ca^{2+}]$ evoked by bAPs (P < 0.01, n = 10)(Fig. 5A1,B1) and by LTS in both proximal (P < 0.001) and distal (P < 0.01)(Fig. 5A2,B2) dendrites without significant changes in $\Delta[Ca^{2+}]$ amplitude (P > 0.05). Consequently, the increase in

τ_{decay} of single bAP evoked transients by SERCA inhibition also resulted in significantly (P < 0.01) larger Ca^{2+} accumulations during 50 Hz (700 ms) trains of APs (Fig. S4).

LTS evoked dendritic Ca^{2+} transients are mediated by T-type Ca^{2+} channels

Global dendritic Ca^{2+} influx during LTS is not reliant, to a large extent, upon actively backpropagating Na^+ mediated APs. To test the hypothesis that $\Delta[Ca^{2+}]_{LTS}$ requires dendritic propagation of LTS and Ca^{2+} influx through T-type channels, we used the novel, potent and highly selective antagonist TTA-P2 (Dreyfus et al., 2010). Bath application of TTA-P2 (10 μM) abolished both somatically evoked LTS and their corresponding dendritic $\Delta[Ca^{2+}]$ (P < 0.001, n = 8, paired t-test)(Fig. 6C1) whilst having no effect upon the Ca^{2+} signal evoked by a train of bAPs (30 Hz, P > 0.05, n = 8)(Fig. 6B,C2). Moreover, injection of large currents into the soma (300 pA, 50 ms), sufficient to passively depolarise neurons to a level similar to that achieved during an LTS, did not evoke $\Delta[Ca^{2+}]$ at dendritic locations less than 30 μm from the soma when T-type channels were blocked (Fig. 6A). This confirmed the absolute requirement of T-type Ca^{2+} channels for active propagation of LTS into dendrites. To investigate the presence of T-type channels in distal dendrites and assess their contribution to $\Delta[Ca^{2+}]_{LTS}$ TTA-P2 was applied focally using a 'puffer' patch pipette placed adjacent (~ 15 μm) to a selected distal dendrite (Fig. 6D). This allowed selective block of T-type channels in a relatively short length of the dendrite of interest whilst preserving the ability to somatically initiate LTS. In these experiments, somatically elicited distal $\Delta[Ca^{2+}]_{LTS}$ were markedly reduced by puffed application of the drug (84.6 ± 3.5 %, P < 0.001, n = 7, paired t-test)(Fig. 6E2,F). In contrast, the somatic voltage signal was unaltered in the presence of TTA-P2 confirming that T-type channels outside the focal region were still able to generate LTS. Importantly, LTSs still evoked $\Delta[Ca^{2+}]_{LTS}$ in distal dendrites contralateral (> 150 μm away) to the dendrite to which TTA-P2 was applied (Fig. 6E3).

Local distal synaptic excitation induces global dendritic Ca^{2+} accumulations

Finally, we determined whether LTSs triggered by distal synaptic excitation were able to evoke global Ca^{2+} signals similar to those produced by somatic current injection. CT afferents were focally stimulated by placing a glass electrode adjacent (< 15 μm) to a selected distal dendrite and delivering brief low intensity stimuli (200 μs, 1-10 V). Delivery of three subthreshold stimuli with varying interstimulus intervals in the presence of the GABA$_A$ blocker SR95531 (10 μM), resulted in facilitation of EPSP amplitude (Fig. 7A,B1). When the ISI was sufficiently short (30 ms), electrical stimulation resulted in significant facilitation of EPSPs ($2^{nd}/1^{st}$ EPSP amplitude 2.28 ± 0.50, P < 0.01, n = 5, repeated measures ANOVA)(Fig. 7B2), as previously shown *in vitro* (Turner and Salt, 1998; Pedroarena and Llinas, 2001) thus confirming selective activation of CT fibres. Furthermore, the first EPSP amplitude was typically small (1.33 ± 0.15 mV) suggesting that our synaptic stimulations involved activation of perhaps only a few CT terminals. In hyperpolarised TC neurons (< −70 mV), increasing stimulus intensity sufficiently to evoke an LTS, resulted in $\Delta[Ca^{2+}]$ being observed at both proximal (20-30 μm) and distal (> 100 μm) locations on dendrites contralateral (> 150 μm away) to the stimulated region (Fig. 7D2,E2). Synaptically evoked $\Delta[Ca^{2+}]_{LTS}$ at both proximal and distal locations had amplitudes that were not significantly (P > 0.05, unpaired t-test) different to those evoked by somatic current injection as well as similar τ_{decay} (Fig. 7E3). In contrast, when neurons were depolarised and single bAPs were synaptically evoked, $\Delta[Ca^{2+}]$ were only observed on proximal contralateral dendrites and not at distal locations (Fig. 7D1,E1). These results suggest that regardless of where they are initiated, regenerative LTSs force the entire TC neuron dendritic arbor to behave as an all-or-none Ca^{2+} signalling unit.

Discussion

The major finding of this study is that both spatial and temporal dynamics of intrinsic dendritic Ca^{2+} signalling in TC neurons are determined in a behavioural state-dependent manner. Thus, LTSs, that are predominantly associated with slow wave sleep (e.g. 1-4 Hz δ waves, <1 Hz slow oscillations) and anaesthesia (Crunelli and Hughes, 2010), can actively propagate throughout the entire dendritic tree of TC neurons permitting near instantaneous *global* Ca^{2+} influx that requires dendritic T-type Ca^{2+} channel expression. Indeed, for the first time, we have demonstrated the presence of T-type Ca^{2+} channels in fine intermediate/ distal TC neuron dendrites and their recruitment by CT synaptic inputs. In clear contrast, APs typical of TC output during wakefulness evoke significantly smaller Ca^{2+} influxes that temporally summate to produce Ca^{2+} accumulations that are linearly related to firing frequency but are spatially restricted to more proximal dendritic regions.

The placement of T-type channels throughout the entire dendritic tree may have several implications for signalling in TC neurons. Firstly, it could allow graded and more subtle modulation of bursts by synaptic currents, in particular by distal modulatory CT EPSPs. For example, distal dendritic placement of these channels may be required to allow phosphorylation-dependent potentiation of I_T in response to corticofugal inputs, thus enhancing burst probability and temporal precision of burst associated AP firing (Bessaïh et al., 2008). Secondly, since TC neuron dendrites are also extensively covered by GABAergic nRT terminals, co-localization of T-type channels with these inhibitory synapses may enhance the genesis of rebound bursts in response to IPSPs. Thirdly, dendritic distribution of T-type Ca^{2+} channels (along with Na^+ and K^+ channels (Williams and Stuart, 2000)) may permit finer and more spatially specific modulation by neuromodulatory systems (i.e. cholinergic brainstem inputs) either directly or through modulation of other dendritic voltage dependent channels (i.e. hyperpolarization activated cation current, I_h or voltage activated K^+ channels). Finally, dendritic LTS propagation may produce global resetting of synaptic integration by shunting effects on membrane resistance. This is particularly interesting in light of the fact that LTSs are not exclusively reserved for periods of sleep but are also, albeit rarely, detected during wakefulness (Guido and Weyand 1995; Reinagel et al., 1999; Alitto et al., 2005).

Our data demonstrates that Ca^{2+} clearance in TC neuron dendrites, both proximally and distally, during LTS relies in part upon net uptake of Ca^{2+} into intracellular stores via SERCA. Coupled with other putative Ca^{2+} clearance mechanisms such as Na^+/Ca^{2+} exchangers and/or plasma membrane Ca^{2+}-ATPases (PMCA), expression of SERCA throughout TC neuron dendrites contributes to rapid decay of global LTS evoked Ca^{2+} signals. Interestingly, in our experiments τ_{decay}, and thus Ca^{2+} extrusion rates, in proximal TC neuron dendrites were strikingly similar during both evoked LTSs and bAPs (single or trains) suggesting that buffering and extrusion mechanisms operate at comparable levels during both state-dependent firing modes. Significantly, such fast extrusion of Ca^{2+} during LTSs coupled with the refractoriness of $Ca_V3.1$ T-type Ca^{2+} channels is likely to permit global dendritic Ca^{2+} oscillations during rhythmic LTS activity at low frequencies. In fact, in the absence of added Ca^{2+} buffer we expect that τ_{decay} of LTS evoked $\Delta[Ca^{2+}]$ would be markedly faster than reported here (~180 ms in proximal dendrites with Fluo 5F), thus resulting in very little (if any) temporal summation of $\Delta[Ca^{2+}]$ during repetitive LTSs at up to ~4 Hz (the upper range of intrinsic δ oscillations). In fact, in distal dendrites, even accounting for possible errors in our measurements due to uneven Ca^{2+} indicator distribution, it seems that Ca^{2+} extrusion is more rapid than at proximal dendritic locations. This may be important because the local amplitude and time course of Ca^{2+} signals can be critical in determining dynamic modulation of Ca^{2+}-dependent signalling processes. For example, repetitive Ca^{2+} influx through T-type channels has been shown to result in

increased cAMP production and a dynamic upregulation of I_h that contributes to periodicity and termination of spindle wave activity (Luthi and McCormick, 1998, 1999). Furthermore, in nRT neurons T channel mediated rhythmic dendritic Ca^{2+} influx can shape oscillatory activity through a dynamic interaction with Ca^{2+}-dependent small conductance potassium channels (SK2) and SERCAs (Cueni et al., 2008).

We have shown that during prolonged AP firing, TC neuron dendrites experience sustained activity-dependent rises in intracellular $[Ca^{2+}]$. The near instantaneous Ca^{2+} influx produced by single bAPs and lack of effect of T-type channel block indicate that these train evoked Ca^{2+} accumulations are mediated by HVA Ca^{2+} channels as have previously been identified in TC neuron proximal dendrites (Zhou et al., 1997; Budde et al., 1998; Munsch et al. 1997; Williams and Stuart, 2000). The precise magnitude of Ca^{2+} accumulation in TC neuron dendrites during AP firing is largely dependent upon two critical factors. Firstly, and in marked contrast to $\Delta[Ca^{2+}]_{LTS}$, we found that the size of dendritic $\Delta[Ca^{2+}]$ produced by actively bAPs or bAP trains was greatly influenced by distance from the soma. This finding can be explained by the failure of bAPs to invade intermediate and distal dendrites owing to the extensively branched morphology of TC neurons and a significant reduction in dendritic Na^+ channel density (Williams and Stuart, 2000), although heterogenous expression of HVA Ca^{2+} channels may also contribute. Secondly, the extent of Ca^{2+} build-up was governed by linear summation of single bAP evoked $\Delta[Ca^{2+}]$ and thus linearly related to AP firing across a wide range of physiologically pertinent frequencies. Under our conditions, activity-dependent linear accumulation of Ca^{2+} coupled with activity-independent Ca^{2+} extrusion rates during AP trains and lack of effect of intracellularly applied ryanodine demonstrates that CICR from internal stores does not contribute to dendritic Ca^{2+} signals as has been suggested by others (Budde et al., 2000, see supplemental material). Indeed, our study places the role of SERCA and the involvement of CICR in intrinsic dendritic Ca^{2+} signalling in TC neurons in line with studies in other neuronal types, including CA1 hippocampal pyramidal neurons (Scheuss et al., 2006), neocortical pyramidal neurons (Markram et al., 1995) and fast spiking interneurons of cortical layer V (Goldberg et al., 2003).

Since bAPs can act as retrograde messengers providing vital information to the input to a neuron (i.e. the synapse) about the status of the cells output, understanding the extent of AP backpropagation and distribution of subsequent Ca^{2+} signals is of considerable importance. This is particularly fascinating in TC neurons because of the preferential innervation of proximal and intermediate/distal dendrites by sensory and CT afferents, respectively, as well as the differential dendritic distribution of GABAergic afferents from local interneurons and the nRT (Sherman and Guillery, 1996; Wilson et al., 1984; Liu et al., 1995). Our results suggest that in TC neurons, bAPs may exercise a greater influence over (and conversely be influenced by) those synaptic inputs that are distributed upon proximal dendrites compared with those found on more distal portions of the cell. For example, bAP mediated dendritic $\Delta[Ca^{2+}]$ may provide a mechanism that allows co-incidence detection at proximal sensory but not distal CT synapses. This may be necessary for robust relay of sensory information or in determining receptive field properties. Furthermore, in contrast to global LTS signals, decrementing AP backpropagation may permit spatially restricted resetting of synaptic integration thus allowing distal processing of modulatory CT inputs to proceed uninfluenced by neuronal output. This has been previously proposed as a mechanism to allow parallel processing of spatially segregated inputs (Häusser et al., 2000) such as the two major glutamatergic afferents found in TC neurons. Finally, frequency-dependent linear Ca^{2+} build up during sustained AP firing at physiologically relevant rates, suggests that $[Ca^{2+}]$ can dynamically encode spike frequency providing a biochemical feedback signal that could control dendritic activity-dependent processes in a spatially graded manner. Indeed, since we predict τ_{decay} for AP evoked $\Delta[Ca^{2+}]$ would be <100 ms in the absence of exogenous Ca^{2+}

buffers (see Fig. 4) our results suggest that changes in firing rate could be rapidly detected by this dendritic 'Ca^{2+} code' in TC neurons (Helmchen, 2008).

Supplementary Material

Refer to Web version on PubMed Central for supplementary material.

Acknowledgments

References

Alitto HJ, Weyand TG, Usrey WM. Distinct properties of stimulus-evoked bursts in the lateral geniculate nucleus. J Neurosci. 2005; 25:514–523. [PubMed: 15647497]

Bessaïh T, Leresche N, Lambert R. T current potentiation increases the occurrence and temporal fidelity of synaptically evoked burst firing in sensory thalamic neurons. Proc Natl Acad Sci USA. 2008; 105(32):11376–11381. [PubMed: 18685097]

Bischofberger J, Jonas P. Action potential propagation into the presynaptic dendrites of rat mitral cells. J Physiol. 1997; 504(2):359–365. [PubMed: 9365910]

Budde T, Munsch T, Pape H-C. Distribution of L-type calcium channels in rat thalamic neurons. Eur J Neurosci. 1998; 10:2309–2321. [PubMed: 9749759]

Budde T, Sieg F, Braunewell K-H, Gundelfinger E, Pape H-C. Ca^{2+}-induced Ca^{2+} release supports the relay mode of activity in thalamocortical cells. Neuron. 2000; 26:483–492. [PubMed: 10839366]

Crunelli V, Hughes SW. The slow (< 1Hz) rhythm of non-REM sleep: a dialogue between three cardinal oscillators. Nat Neurosci. 2010; 13(1):1392–1398.

Cueni L, Canepari M, Luján R, Emmenegger Y, Watanabe M, Bond CT, Franken P, Adelman JP, Lüthi A. T-type Ca2+ channels, SK2 channels and SERCAs gate sleep-related oscillations in thalamic dendrites. Nat Neurosci. 2008; 11(6):683–692. [PubMed: 18488023]

Destexhe A, Neubig M, Ulrich D, Huguenard J. Dendritic low-threshold calcium currents in thalamic relay cells. J Neurosci. 1998; 18(10):3574–3588. [PubMed: 9570789]

Dreyfus F, Tscherter A, Errington AC, Renger JJ, Shin HS, Uebele VN, Crunelli V, Lambert RC, Leresche N. Selective T-type calcium channel block in thalamic neurons reveals channel redundancy and physiological impact of I$_{Twindow}$. J Neurosci. 2010; 6(30):99–109. [PubMed: 20053892]

Emri Z, Antal K, Tóth TI, Cope DW, Crunelli V. Backpropagation of the δ oscillation and the retinal excitatory post synaptic potential in a multi-compartment model of thalamocortical neurons. Neuroscience. 2000; 98(1):111–127. [PubMed: 10858617]

Guido W, Weyand T. Burst responses in thalamic relay cells of the awake behaving cat. J Neurophysiol. 1995; 74:1782–1786. [PubMed: 8989413]

Häusser M, Stuart G, Racca C, Sakmann B. Axonal initiation and active dendrtic propagation of action potentials in substantia nigra neurons. Neuron. 1995; 15:637–647. [PubMed: 7546743]

Häusser M, Spruston N, Stuart GJ. Diversity and dynamics of dendritic signalling. Science. 2000; 290:739–744. [PubMed: 11052929]

Helmchen F, Imoto K, Sakmann B. Ca^{2+} buffering and action potential-evoked Ca^{2+} signalling in dendrites of pyramidal neurons. Biophys J. 1996; 70:1069–1081. [PubMed: 8789126]

Helmchen, F. Dendrites. 2nd Ed.. Stuart, GJ.; Spruston, N.; Häusser, M., editors. Oxford University Press; Oxford, UK: 2008. p. 278-279.

Holthoff K, Kovalchuk Y, Konnerth A. Dendritic spikes and activity-dependent synaptic plasticity. Cell Tissue Res. 2006; 326(2):369–377. [PubMed: 16816965]

Kampa B, Stuart GJ. Calcium spikes in basal dendrites of layer 5 pyramidal neurons during action potential bursts. J Neurosci. 2006; 26(28):7424–7432. [PubMed: 16837590]

Kampa BM, Letzkus JJ, Stuart GJ. Dendritic mechanisms controlling spike-timing-dependent synaptic plasticity. TINS. 2007; 30:456–463. [PubMed: 17765330]

Larkum ME, Kaiser KM, Sakmann B. Calcium electrogenesis in distal apical dendrites of layer 5 pyramidal cells at a critical frequency of back-propagating action potentials. Proc Natl Acad Sci USA. 1999; 96:14600–14604. [PubMed: 10588751]

Larkum ME, Waters J, Sakmann B, Helmchen F. Dendritic spikes in apical dendrites of neocortical layer 2/3 pyramidal neurons. J Neurosci. 2007; 27(34):8999–9008. [PubMed: 17715337]

Liu X-B, Honda CN, Jones EG. Distribution of four types of synapse on physiologically identified relay neurons in the ventral posterior thalamic nucleus of the cat. J Comp Neurol. 1995; 414:67–69. [PubMed: 10494079]

Llinas R, Jahnsen H. Electrophysiology of mammalian thalamic neurons in *vitro*. Nature. 1982; 297:406–408. [PubMed: 7078650]

Lüthi A, McCormick D. Periodicity of thalamic synchronized oscillations: the role of Ca^{2+} mediated upregulation of I_h. Neuron. 1998; 20:553–563. [PubMed: 9539128]

Lüthi A, McCormick D. Modulation of a pacemaker current through Ca^{2+}-induced stimulation of cAMP production. Nat Neurosci. 1999; 2(7):634–641. [PubMed: 10404196]

Magee JC, Johnston D. Synaptic activation of voltage-gated channels in dendrites of hippocampal pyramidal neurons. Science. 1995; 268:301–304. [PubMed: 7716525]

Markram H, Helm PJ, Sakmann B. Dendritic calcium transients evoked by single back-propagating action potentials in rat neocortical pyramidal neurons. J Physiol. 1995; 485:1–20. [PubMed: 7658365]

Munsch T, Budde T, Pape H-C. Voltage-activated intracellular calcium transients in thalamic relay neurons and interneurons. Neuroreport. 1997; 8:2411–2418. [PubMed: 9261800]

Neher E, Augustine GJ. Calcium gradients and buffers in bovine chromaffin cells. J Physiol. 1992; 450:273–301. [PubMed: 1331424]

Pedroarena C, Llinas R. Interactions of synaptic and intrinsic electroresponsiveness determine corticothalamic activation dynamics. Thal Rel Sys. 2001; 1:3–14.

Reinagel P, Godwin D, Sherman SM, Kock C. Encoding of visual information by LGN bursts. J Neurophysiol. 1999; 81:2558–2569. [PubMed: 10322089]

Rhodes PA, Llinas R. A model of thalamocortical relay cells. J Physiol. 2005; 565:765–781. [PubMed: 15613378]

Scheuss V, Yasuda R, Sobczyk A, Svoboda K. Nonlinear [Ca^{2+}] signalling in dendrites and spines caused by activity-dependent depression of Ca^{2+} extrusion. J Neurosci. 2006; 26(31):8183–8194. [PubMed: 16885232]

Schiller J, Helmchen F, Sakmann B. Spatial profile of dendritic calcium transients evoked by action potentials in rat neocortical neurones. J Physiol. 1995; 487:583–600. [PubMed: 8544123]

Sherman SM, Guillery RW. Functional organization of thalamocortical relays. J Neurophysiol. 1996; 76:1367–1395. [PubMed: 8890259]

Spruston N, Schiller Y, Stuart GJ, Sakmann B. Activity-dependent action potential invasion and calcium influx into hippocampal CA1 dendrites. Science. 1995; 268:297–300. [PubMed: 7716524]

Steriade M, McCormick D, Sejnowski TJ. Thalamocortical oscillation in the sleeping and aroused brain. Science. 1993; 262:679–685. [PubMed: 8235588]

Stuart GJ, Dodt HU, Sakmann B. Patch-clamp recordings from the soma and dendrites of neurons in brain slices using infrared video microscopy. Pflügers Arch. 1993; 423:511–518.

Stuart GJ, Schiller J, Sakmann B. Action potential initiation and propagation in rat neocortical pyramidal neurons. J Physiol. 1997; 505(3):617–632. [PubMed: 9457640]

Turner JP, Salt TE. Characterization of sensory and corticothalamic excitatory inputs to rat thalamocortical neurones *in vitro*. J Physiol. 1998; 510(3):829–843. [PubMed: 9660897]

Williams SR, Stuart GJ. Action potential backpropagation and somato-dendritic distribution of ion channels in thalamocortical neurons. J. Neurosci. 2000; 20(4):1307–1317. [PubMed: 10662820]

Wilson JR, Friedlander MJ, Sherman SM. Fine structural morphology of identified X- and Y-cells in the cat's lateral geniculate nucleus. Proc R Soc Lond. 1984; B221:411–436. [PubMed: 6146984]

Yasuda R, Sabatini BL, Svoboda K. Plasticity of calcium channels in dendritic spines. Nat Neurosci. 2003; 6(9):948–954. [PubMed: 12937422]

Zhou Q, Godwin DW, O'Malley DM, Adams PR. Visualization of calcium influx through channels that shape the burst and tonic modes of thalamic relay cells. J Neurophysiol. 1997; 77:2816–2825. [PubMed: 9163395]
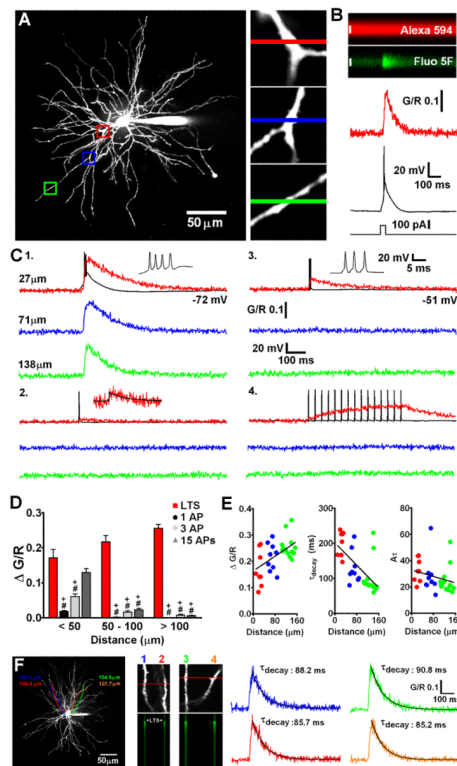
Fig. 1.

State-dependent firing determines differences in spatial distribution of $\Delta[Ca^{2+}]$ in TC neuron dendrites. (A) Maximum intensity projection of a typical dLGN neuron illustrating the dendritic sites (also shown in increased magnification, right) where linescans shown in C were performed. Proximal, intermediate and distal dendritic locations are colour coded red, blue and green respectively. (B) A typical experiment illustrating increase in green fluorescence relative to red fluorescence (G/R) in a TC neuron dendrite resulting from a somatically elicited LTS. (C) Dendritic $\Delta[Ca^{2+}]$ evoked by (1) LTS, (2) single bAP, (3) 3 bAP (200 Hz) burst, and (4) 15 bAPs at 30 Hz are shown overlaid onto somatically recorded voltage traces. A single AP transient is shown enlarged for clarity in 2. Black line represents a mono-exponential fit to the data. (D) Summary of $\Delta[Ca^{2+}]$ amplitudes grouped by dendritic location. *: $P < 0.05$ (vs proximal $\Delta[Ca^{2+}]_{LTS}$), #: $P < 0.001$ (vs proximal $\Delta[Ca^{2+}]_{LTS}$), +: $P < 0.001$ (vs $\Delta[Ca^{2+}]_{LTS}$ for each dendritic location). n = 6-11 cells. (E) $\Delta[Ca^{2+}]$ amplitudes, τ_{decay} and time integrals (Aτ) for LTS evoked signals as a function of distance from the soma. The plot of Aτ versus distance reveals a more uniform distribution suggesting comparable Ca^{2+} influx throughout the entire dendritic tree. (F) Somatically evoked LTSs produce synchronous Ca^{2+} transients throughout the entire dendritic tree. Two different pairs of distal dendrites (100-110 μm from the soma) lying in the same focal plane but originating from different stem dendrites (coloured tracings constructed from 3D Z-series) were imaged separately during evoked LTS activity. In both pairs of dendrites $\Delta[Ca^{2+}]_{LTS}$ occurred simultaneously and in all four dendrites the amplitude and τ_{decay} of the evoked Ca^{2+} transients were identical (n = 4 dendrite pairs from 3 neurons).
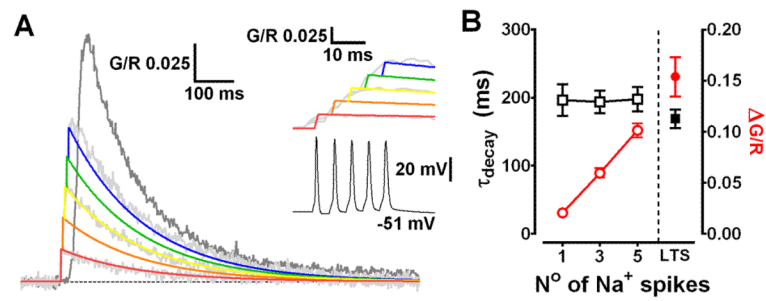
Fig. 2.
LTS produce supralinear dendritic $\Delta[Ca^{2+}]$ (A) Traces depicting the linear summation of $\Delta[Ca^{2+}]$ evoked by 1, 3 and 5 bAPs (light grey) compared to $\Delta[Ca^{2+}]_{LTS}$ (dark grey) in proximal TC neuron dendrites (20-30 μm). Coloured lines represent the modelled linear sum of single bAP $\Delta[Ca^{2+}]$ (red) offset for spike timing. (B) Plot of amplitude (red) and τ_{decay} (black) for $\Delta[Ca^{2+}]$ evoked by bAP (200 Hz) and LTS in the same neurons (n = 11).
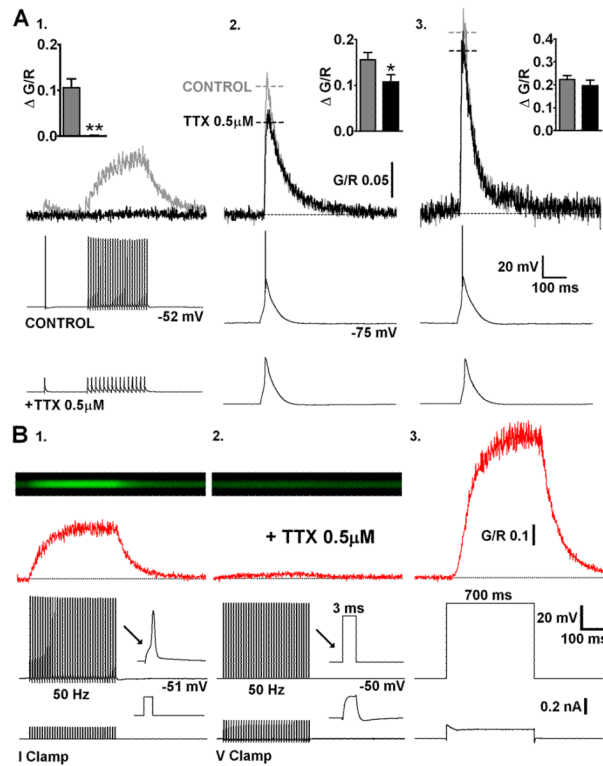
Fig. 3.
LTS evoked dendritic $\Delta[Ca^{2+}]$ are largely AP independent. (A) Representative $\Delta[Ca^{2+}]$ (top) evoked in a proximal TC neuron dendrite before (grey) and after (black) bath application of TTX (bottom). (1) bAPs (500 ms, 30 Hz) are blocked by TTX along with their corresponding proximal dendritic $\Delta[Ca^{2+}]$. (2) In the absence of Na^+ spike bursts, $\Delta[Ca^{2+}]_{LTS}$ is slightly reduced at proximal dendritic locations. (3) Distal $\Delta[Ca^{2+}]_{LTS}$ is not altered by the addition of TTX. Summary data (n = 9) in inset histograms. (B) (1) In current clamp recording mode, trains of evoked APs produce $\Delta[Ca^{2+}]$ that linearly summate and are blocked by TTX. (2) In voltage clamp recording mode, in the presence of TTX, voltage steps from −50 mV to +10 mV for 3 ms at a frequency of 50 Hz (to mimic AP firing shown in A) failed to elicit significant Ca^{2+} accumulation in proximal (20-30 μm) TC neuron dendrites. (3) In contrast, a 700 ms depolarising step to +10 mV evoked very large Ca^{2+} influx (sufficient to nearly saturate the Ca^{2+} indicator), presumably through direct opening of HVA Ca^{2+} channels.
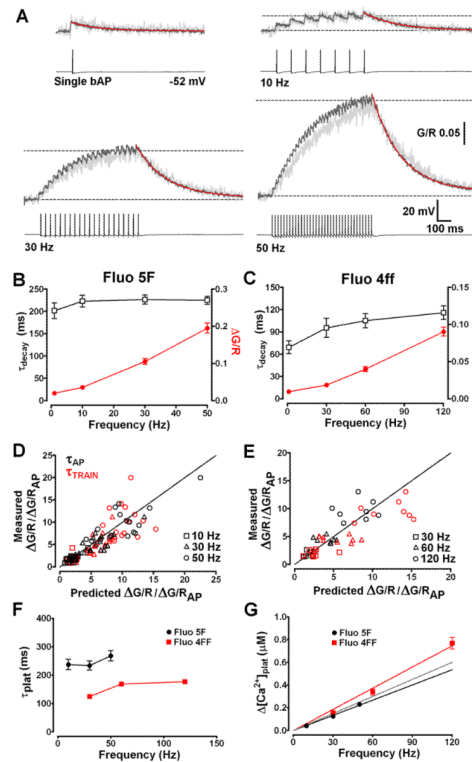
Fig. 4.
Dendritic Ca^{2+} accumulation is linearly related to AP firing frequency. (A) Typical $\Delta[Ca^{2+}]$ evoked in an individual TC neuron proximal dendrite (light grey) by a single bAP and 700 ms spike trains at 10, 30 and 50 Hz (traces truncated for clarity). Overlays (dark grey) show the average $[Ca^{2+}]_{plat}$ pooled from 18 different TC neurons. Decay phases are fitted with mono-exponential functions (red lines) to yield τ_{decay}. Dashed lines show baseline and $[Ca^{2+}]_{plat}$ levels. (B) Summary of τ_{decay} (black open squares) and $\Delta G/R$ (red closed circles) for single bAPs and bAP trains in TC neurons filled with Fluo 5F. τ_{decay} are not significantly ($P < 0.05$) slowed at firing frequencies up to 50 Hz. (C) As in B for Fluo 4ff (500 μM, n = 13). (D) Comparison of measured $[Ca^{2+}]_{plat}$ amplitude for individual neurons versus predicted $[Ca^{2+}]_{plat}$ amplitude based upon the amplitude and τ_{decay} of the $\Delta[Ca^{2+}]$ evoked by a single bAP. Simulations based upon τ_{decay} of single $\Delta[Ca^{2+}]_{bAP}$ (black symbols) or τ_{decay} for each train evoked $[Ca^{2+}]_{plat}$ (red symbols) showed little deviation from equality (black solid line). Under these conditions $[Ca^{2+}]_{plat}$ levels are linearly related to firing frequency. (E) As in D for Fluo 4ff (n = 8). (F) Plot depicting the time constants for Ca^{2+} accumulation to plateau (τ_{plat}) for all frequencies tested. Mono-exponetial fits to the rising phase of trains evoked $\Delta[Ca^{2+}]$ showed little dependency of τ_{plat} upon firing rate in neurons filled with either Fluo 5F (black) or Fluo 4ff (red). In the presence of lower added buffer $\Delta[Ca^{2+}]$ more rapidly reached steady-state levels. (G) $[Ca^{2+}]_{plat}$ is plotted against AP firing frequency for experiments performed using Fluo 5F (K_d: 0.8μM, black circles) and Fluo 4ff (K_d: 8.1μM red squares). Red and black lines represent linear fits to the data for each indicator. The grey line represents a linear fit to the pooled data (excluding 120Hz which showed small non-linearity).
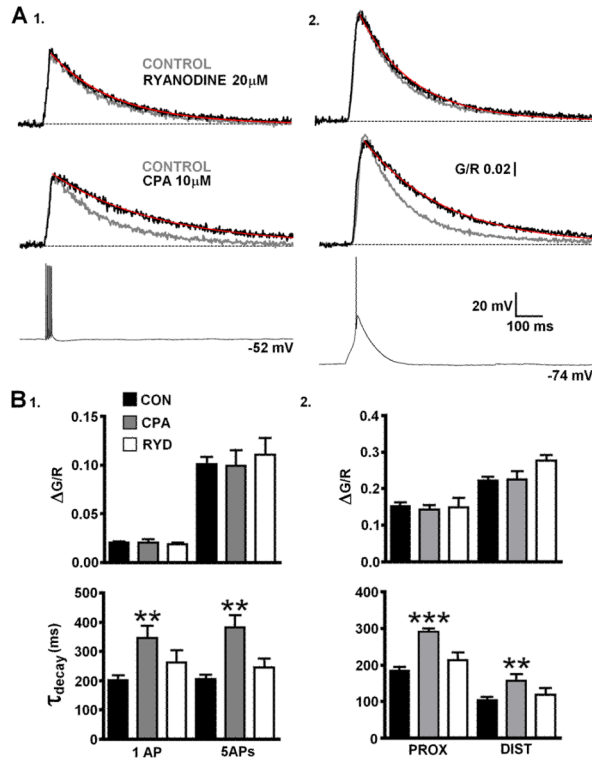
Fig. 5.
Net Ca^{2+} uptake into ER stores by SERCA during LTS and bAP evoked dendritic $\Delta[Ca^{2+}]$.
(A) Amplitudes of $\Delta[Ca^{2+}]$ evoked by (1) a burst of 5 bAPs (200 Hz) or (2) LTS are not
changed by ryanodine (n = 9) or CPA (n = 10) but τ_{decay} is significantly slowed for both in
the presence of the SERCA blocker compared with control (n = 11). Traces represent pooled
averages of $\Delta[Ca^{2+}]$ for each different group of cells. (B) (1) Histograms summarise the
effects of ryanodine and CPA upon amplitude and τ_{decay} of $\Delta[Ca^{2+}]_{bAP}$ or $\Delta[Ca^{2+}]_{5bAPs}$
compared to control neurons (n = 18, single bAPs; n = 11, 5bAPs) in proximal dendrites. (2)
As in 1 for $\Delta[Ca^{2+}]_{LTS}$ in proximal and distal dendrites.
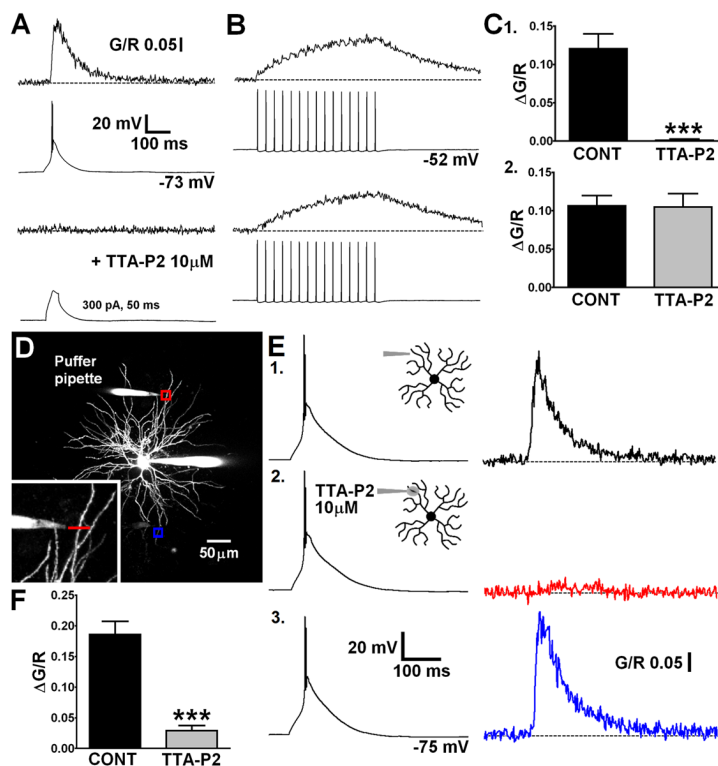
Fig. 6.
Global LTS evoked $\Delta[Ca^{2+}]$ are mediated by dendritic T-type Ca^{2+} channels. (A) LTS were blocked by bath application of TTA-P2 and their corresponding dendritic $\Delta[Ca^{2+}]$ were abolished. Current injection sufficient to produce somatic depolarisation similar in magnitude to LTS could not passively induce increases in dendritic $[Ca^{2+}]$. (B) Action potential trains and their corresponding proximal dendritic $[Ca^{2+}]_{plat}$ were unaffected by TTA-P2. (C) Summary histograms of data in A and B. (D) Maximum intensity Z-projection of a dLGN neuron showing placement of a 'puffer' pipette near a distal dendrite for focal application of TTA-P2. Red and blue boxes correspond to the dendritic regions where linescans shown in E were performed. (E) (1) $\Delta[Ca^{2+}]$ recorded in the dendrite close to the application pipette under control conditions in response to a somatically elicited LTS. (2) During focal application of TTA-P2 the distal $\Delta[Ca^{2+}]$ (red) is blocked without changes to the somatic LTS. (3) The $\Delta[Ca^{2+}]$ in a contralateral dendrite (blue) is unaffected by the focal application of TTA-P2 at > 200 μm away. (F) Summary histogram of data in E1,2.
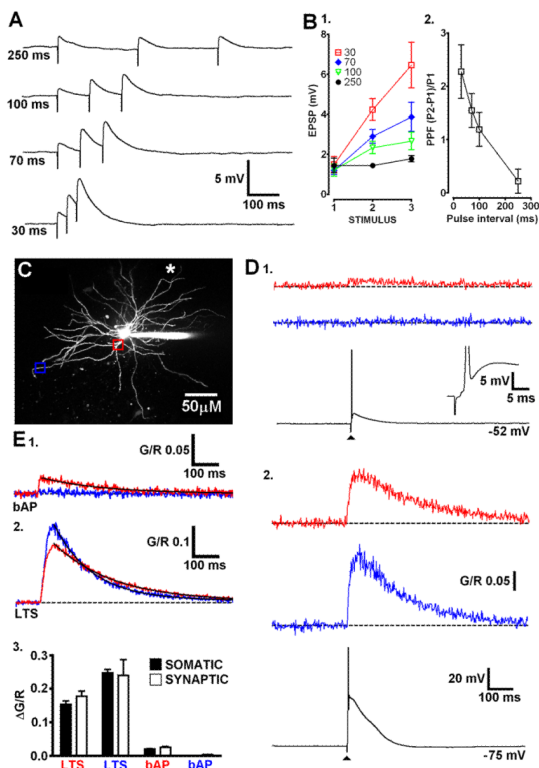
Fig. 7.
Distal synaptic inputs evoke LTS and trigger global dendritic Ca^{2+} influx. (A) Traces depicting EPSPs typical of activation of CT afferents by focal synaptic stimulation close to distal dendrites. Varying degrees of synaptic facilitation are observed at different interstimulus intervals. (B) (1) Summary plot showing the range of interstimulus intervals that produce marked facilitation of synaptic potentials. (2) Plot describing the degree of paired-pulse facilitation between the first two stimuli of each train. (C) Maximum intensity projection of dLGN cell showing proximal (red) and distal (blue) locations imaged on a dendrite contralateral to the stimulated dendrite (white asterisk indicates placement of stimulating electrode). (D) (1) An AP evoked by stimulation of local CT afferents produces Ca^{2+} influx at the proximal dendritic location but not distally. (2) An LTS synaptically triggered from a more hyperpolarised membrane potential evoked Ca^{2+} influx at both proximal and distal locations. (E) Averaged Ca^{2+} transients (n = 5 cells) in proximal (20-30 μm) and distal (> 100 μm) segments of TC neurons resulting from synaptically evoked (1) bAP or (2) LTS. Black lines represent mono-exponential fits to the data. (3) Summary of the experiments depicted in B. Amplitudes of synaptically evoked $\Delta[Ca^{2+}]_{LTS}$ and $\Delta[Ca^{2+}]_{bAP}$ are not significantly different to those produced by somatic current injection (n = 5-9, P > 0.05, unpaired t-test).